Electro-Elastic Modeling of Multi-Step Transitions in Two Elastically Coupled and Sterically Frustrated 1D Spin Crossover Chains

Rachid Traiche, Hassane Oubouchou, Kamel Boukheddaden

crystals

MDPI

Article

Electro-Elastic Modeling of Multi-Step Transitions in Two Elastically Coupled and Sterically Frustrated 1D Spin Crossover Chains

Rachid Traiche [1,*], Hassane Oubouchou [2] and Kamel Boukheddaden [3,*]

[1] Laboratoire de Physique Théorique et de Physique des Matériaux LPTPM, BP 151 Hay Salem, Chlef 02000, Algeria
[2] Laboratoire des Diélectriques, Université Houari Boumedienne, BP 32 El Alia Bab Ezzouar, Alger 16111, Algeria; h.oubouchou@epau-alger.edu.dz
[3] Groupe d'Etudes de la Matière Condensée, Université de Versailles-Saint-Quentin Paris-Saclay, UMR CNRS, 8635, 45 Avenue des Etats Unis, 78035 Versailles, France
* Correspondence: r.traiche@univ-chlef.dz (R.T.); kamel.boukheddaden@uvsq.fr (K.B.)

Abstract: One-dimensional spin crossover (SCO) solids that convert between the low spin (LS) and the high spin (HS) states are widely studied in the literature due to their diverse thermal and optical characteristics which allow obtaining many original behaviors, such as large thermal hysteresis, incomplete spin transitions, as multi-step spin transitions with self-organized states. In the present work, we investigate the thermal behaviors of a system of two elastically coupled 1D mononuclear chains, using the electro-elastic model, by including an elastic frustration in the nearest neighbors (nn) bond length distances of each chain. The chains are made of SCO sites that are coupled elastically through springs with their nn and next-nearest neighbors. The elastic interchain coupling includes diagonal springs, while the nn inter-chain distance is fixed to that of the high spin state. The model is solved using MC simulations, performed on the spin states and the lattice distortions. When we only frustrate the first chain, we found a strong effect on the thermal dependence of the HS fraction of the second chain, which displays an incomplete spin transition with a significantly lowered transition temperature. In the second step, we frustrate both chains by imposing different frustration rates. Here, we demonstrate that for high frustration values, the thermal dependence of the total HS fraction exhibits multi-step spin transitions. The careful examination of the spin state structures in the plateau regions showed the coexistence of special dimerized ferro–antiferro patterns of type LL-HH-LL-HH along the first chain and HH-LL-HH-LL (H=HS and L=LS) along the second one, revealing that the two chains are antiferro-elastically coupled. This type of spatial modulation of the spin state and bond length distances is very attractive because it anticipates the possible existence of periodic structures in 2D lattices, made of alternate 1D SCO strings with HLHLHL structures, coupled in the ferro-like fashion along the interchain direction.

Keywords: spin crossover; phase transition; elastic frustration; Monte Carlo simulations; elastic models

Citation: Traiche, R.; Oubouchou, H.; Boukheddaden, K. Electro-Elastic Modeling of Multi-Step Transitions in Two Elastically Coupled and Sterically Frustrated 1D Spin Crossover Chains. *Crystals* **2023**, *13*, 937. https://doi.org/10.3390/cryst13060937

Received: 20 April 2023
Revised: 2 June 2023
Accepted: 6 June 2023
Published: 10 June 2023

1. Introduction

Spin crossover (SCO) materials represent a fascinating generation of switchable molecular solids, offering serious applications, in molecular electronics, for the development of new devices, such as molecular sensors, displays, nonvolatile memories, and reversible switches [1–5]. Among them, the most studied objects are iron (II)-based SCO solids [1,5–9], characterized by their labile electronic character, which confers them the interesting property to convert from a diamagnetic low spin state $(\mathrm{LS}, e_g^0 t_{2g}^6, S = 0)$ to a paramagnetic high spin state $(\mathrm{HS}, e_g^2 t_{2g}^4, S = 2)$ upon change of an external stimulus, such as temperature, pressure [10], light [11–15], static and pulsed electric [16,17] and magnetic fields [18]. The SCO phenomenon is therefore generally possible when the central metal ion (here iron) is

surrounded by nitrogen atoms in octahedral symmetry. This is the situation that fulfills the requirement of energetic balance between the ligand field energy, originating from the nitrogen environment, and the electronic pairing energy in the d orbitals. When these energies have the same order of magnitude as the thermal energy, k_BT, the SCO phenomenon may take place.

At the molecular level, the change of the spin state of the Fe along the spin transition is accompanied by a volume change of the coordination sphere by about 30%, as a result of the change of the Fe-ligand distances by almost 10% [5]. However, it is important to notice that a significant part of this molecular volume change is absorbed by the lattice through ligand rotations and elastic relaxations in such a way that only 3% of volume expansion/contraction is observed at the scale of the unit cell. Although these changes occur at the molecular scale, they easily delocalize over the whole crystal through elastic strain, mediated by acoustic phonons, leading to long-range elastic interactions [19], which are predominant in most SCO materials. From the experimental point of view, the thermally-induced SCO transition may appear through several types: (i) continuous spin transitions [20], (ii) discontinuous first-order transitions [21], and (iii) incomplete transitions [22] with residual HS fractions and (iv) multi-step spin transitions [23–26]. On this latter point especially, it is worth noticing that several recent works [27–32] demonstrated the occurrence of competing elastic interactions in SCO lattices, termed elastic frustration in a theoretical concept that was introduced by Paez-Espejo et al. [33] in 2016.

This concept is at the heart of the thermodynamic nature of the spin transition and allows to build a global view of all the experimental thermal dependencies of the high spin fraction. Thus, the absence or weakness of elastic frustration, combined with a significant ferro-elastic coupling, often leads to abrupt thermal hysteresis favoring the emergence of a bistability situation, which is highly sought after for reversible memory applications. The latter also allows the switching of a set of physical properties of different natures: magnetic, mechanical, optical, etc. On the other hand, the presence of a significant elastic frustration, which may be due to steric effects, originating from the surrounding ligands or induced by an additional degree of freedom of the counterions (rotation, displacement) creating either isotropic or anisotropic elastic stress, leads to the emergence of multi-step transitions on the thermal dependence of the HS fraction. At the microscopic scale, these steps reveal most often the existence of quite fascinating electronic and structural self-organizations, giving rise to the coexistence of spatial organization of HS and LS phases often similar to charge density waves. In this context, it is important to recall that in some incomplete spin transitions, commensurate/incommensurate structures between the spatial change of the lattice parameter and that of the spin state have been also revealed [34,35], and attributed to elastic frustration effects, which are most often accompanied by symmetry breaking in the plateaus regions. Furthermore, most of the observations dealing with elastic frustration in SCO materials were reported for 2D [36] and 3D materials, although some of them also concerned SCO materials with a strong 1D character [29]. From the theoretical point of view, several models have been developed to describe the multi-step transitions in SCO solids. The most famous are based on the Ising-like models combining competing ferro- and antiferro-like exchange interactions [37,38], which were solved using mean-field theory or Monte Carlo (MC) simulations. Later on, more sophisticated models, based on an electro-elastic description of the SCO lattices, addressed the issue of the multi-step transitions through the concept of elastic frustration, resulting from the presence of antagonist steric effects. The first work bringing this idea was reported in Ref [36], where the authors studied the effect of an elastic frustration injected along the diagonals in a 2D elastic lattice, made of fictitious spins coupled by springs. This idea was developed and applied to several situations, among which are the cases of (i) core–shell SCO nanoparticles [39], (ii) SCO materials deposited on a substrate [40], and (iii) mechanically constrained SCO lattices [41].

In a recent work [42], this model was adapted for the analysis of the frustration effects on the thermal properties of 1D isolated SCO chains. In this specific case, the frustration was injected in the equilibrium distance of the next-nearest neighbors (nnn) sites which was

taken so as to be incompatible with that of the nearest neighbors (nn) sites along the chain. Here, we found that these simple ingredients are sufficient to generate first-order and multi-step transitions with plateaus in which antiferro-like (HLHL) organizations of the spin states are produced. This work was extended in Ref. [43] to the case of an isolated 1D binuclear chain, where each molecule is now made of two SCO atoms, forming a dinuclear unit. In this case, one has to consider intra- and inter-molecular elastic interactions between the dinuclear species. In the latter case, the elastic frustration is injected in the intra-dinuclear equilibrium distance, where usually the chemical bonds are more rigid than those of the inter-binuclear ones, which generally involve weak van der Waals interactions.

In the present contribution, we extend the 1D electro-elastic model [42] to explore the effect of an elastic frustration in a system made of two elastically coupled 1D SCO chains, each containing $N = 120$ sites. For simplicity, the two chains are also coupled along their diagonal directions and the shortest distance between sites facing each other is maintained constant to reduce the number of model parameters. In a similar way to that of Ref. [42], the frustration is implemented only inside the nn equilibrium bond lengths, while those of the nnn are maintained free from additional stress. In the following simulations, the frustration will be considered either in one chain to study its effect on the other chain, or in both chains to investigate the interplay and the elastic interferences induced by two coupled chains having different elastic frustration rates. As in the previous studies, the simulations are performed using the MC method running on spins and lattice positions accounting for the change of the chain size along the spin transition.

The manuscript is organized as follows. Section 2 introduces the model Hamiltonian and the details of the simulations. In Section 3.1, we present the results in the case of only one frustrated chain. In Section 3.2, we frustrate both chains and study their thermal properties for various frustrations rates. In Section 4 we conclude and outline some possible extensions of the present model.

2. The 1D Electro-Elastic Model

We consider a model system, made of two elastically-frustrated 1D SCO chains, each one containing $N = 120$ SCO sites. The sites inside each chain are connected by nn and nnn springs, while the interchain elastic interactions are ensured by diagonal springs, as depicted in Figure 1. In each chain, the atoms (sites) can occupy two states, namely low spin (LS) and high spin (HS), to which we associate the fictitious spin state, S, whose eigenvalues are, respectively, $S = -1$ (LS) and $S = +1$ (HS).

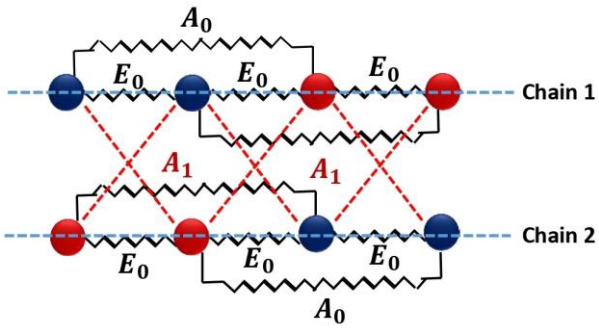

Figure 1. Schematic view of the interaction configurations of selected sites among the two 1D coupled SCO chains, considered in this study.

2.1. The Model Hamiltonian without Frustration

In the current model, the lattice sites are coupled by springs and are constrained to move only along the direction of the chains (i.e., x-direction). Thus, the atoms do not move along the y-direction where the shortest distance between the two chains (along the y-direction) is fixed to $R_0^{HH} = 1.2$ nm. In each chain, the sites are coupled elastically to their nn by springs of elastic constant E_0 and to their nnn by other springs of elastic constant, A_0. The elastic interchain interaction is ensured by diagonal springs of elastic constant A_1. The

equilibrium distances between the SCO sites depend on the values of the spin states of the linked sites, as it will be detailed below. Figure 1 summarizes all information concerning the configuration scheme of the intra- and inter-chain elastic interactions.

As described above, the equilibrium bond lengths between the sites depend on the spin states of the connected sites. This important property allows to include the change of the length of the chain along the spin transition between the LS and the HS states. Thus, the equilibrium distances between two nn sites i and $i+1$ are noted $R(S_{1,i}, S_{1,i+1})$, for the first (top) chain numbered by index 1, and $R(S_{2,i}, S_{2,i+1})$ for the second (bottom) chain numbered by index 2. To use a more compact form for the expressions of the equilibrium intra-chain bond lengths as a function of the fictitious spin states of nn (resp. nnn) i and $i+1$ (resp. i, $i+2$) sites, we adopt the following notation, $R(S_{\ell,i}, S_{\ell,i+1})$ (resp. $R'(S_{\ell,i}, S_{\ell,i+2})$), where $\ell = 1, 2$ stands for the chain number. The expressions of $R(S_{1,i}, S_{1,i+1})$ and $R(S_{2,i}, S_{2,i+1})$ are written so as to ensure a bigger length of the chain in the HS state in comparison to that of the LS state. Between the chains, the equilibrium nn distances are taken equal to R_0^{HH} and those along the diagonal directions, involving spins from both chains, are noted, $D_0(S_{1,i}, S_{2,i+1})$.

The total Hamiltonian describing this system of two coupled 1D chains, accounting for the electronic and elastic degrees of freedom [39,44–47], writes:

$$H = H_1 + H_2 + H_{12}, \tag{1}$$

where, H_1 and H_2 are the respective energetic contributions of chains 1 and 2, while H_{12} accounts for the elastic interaction between the two chains. Their expressions are given as follows:

$$H_1 = \tfrac{1}{2}\sum_{i=1}^{N_x}(\Delta_0 - k_B T \ln g) S_{1,i} + E_0 \sum_{i=1}^{N_x}\left[\left((x_{1,i} - x_{1,i+1}) - R(S_{1,i}, S_{1,i+1})\right)\right]^2 + A_0 \sum_{i=1}^{N_x}\left[\left((x_{1,i} - x_{1,i+2}) - R'(S_{1,i}, S_{1,i+2})\right)\right]^2, \tag{2}$$

$$H_2 = \tfrac{1}{2}\sum_{i=1}^{N_x}(\Delta_0 - k_B T \ln g) S_{2,i} + E_0 \sum_{i=1}^{N_x}\left[\left((x_{2,i} - x_{2,i+1}) - R(S_{2,i}, S_{2,i+1})\right)\right]^2 + A_0 \sum_{i=1}^{N_x}\left[\left((x_{2,i} - x_{2,i+2}) - R'(S_{2,i}, S_{2,i+2})\right)\right]^2, \tag{3}$$

$$H_{12} = \sum_{i=1}^{N_x} A_1 \left[d_{12} - \sqrt{2} D_0(S_{1,i}, S_{2,i\pm1})\right]^2, \tag{4}$$

where, d_{12}=$\sqrt{(x_{2,i+1} - x_{1,i})^2 + \left(R_0^{HH}\right)^2}$(or $\sqrt{\left(x_{1,i} - x_{2,i+1}\right)^2 + \left(R_0^{HH}\right)^2}$) is the instantaneous distance for both diagonal directions between the two chains (red dashed lines in Figure 1.

The first terms in H_1 and H_2 in Equations (2) and (3) correspond to the electronic contributions of the ligand field energy Δ_0 at 0 K, while the temperature-dependent term $-k_B T \ln g$, accounts for the entropic effects originating from the difference of effective electronic and vibrational degeneracies of the LS and the HS states, attributed to the significant changes in intra-molecular vibrations and lattice phonons spectra upon HS to LS transition. The second and the third terms of Hamiltonians H_1 and H_2, describe the elastic interactions between the nn and nnn sites, respectively. Here, the elastic constants E_0 and A_0 are assumed, for simplicity, as independent of spins (S_i) and site positions (x_i).

In the non-frustrated version of the model, the nn (resp. nnn) i and $i+1$ (resp. i and $i+2$) sites of the first chain with corresponding spins $S_{1,i}$ and $S_{1,i+1}$ (resp. $S_{1,i}$ and $S_{1,i+2}$) are linked through springs, whose bond lengths at equilibrium are noted $R_0(S_{1,i}, S_{1,i+1})$ (resp. $R_0'(S_{1,i}, S_{1,i+2})$). The same notation applies for the second chain too.

Let us denote by $R_0^{HH} = R_0(+1, +1)$, $R_0^{LL} = R_0(-1, -1)$, and $R_0^{HL} = R_0(+1, -1)$ the respective nn equilibrium distances between the HS-HS (HH), LS-LS (LL), and HS-LS (HL) sites. Due to the volume increase upon LS to HS transition, one has $R_0^{HH} > R_0^{HL} > R_0^{LL}$. Moreover, for the sake of simplicity, we consider here that, $R_0^{HL} = \frac{R_0^{HH} + R_0^{LL}}{2}$, which means that the equilibrium bond length between two nn HS and LS sites is exactly equal to the average distance between those of LL and HH configurations. Within this framework, it

is quite easy to demonstrate that the general expressions of the nn and nnn equilibrium distances relate to the spin states through the simple general formulas:

$$R_0(S_{\ell,i}, S_{\ell,i+1}) = R_0^{HL} + \frac{\delta_R}{4}(S_{\ell,i} + S_{\ell,i+1}), \tag{5}$$

$$R_0'(S_{\ell,i}, S_{\ell,i+2}) = 2R_0^{HL} + \frac{\delta_R}{2}(S_{\ell,i} + S_{\ell,i+2}), \tag{6}$$

where the quantity $\delta_R = \left(R_0^{HH} - R_0^{LL}\right)$ is the lattice parameter misfit between the pure LS and the HS phases.

Hamiltonian H_{12}, given in Equation (4), which contains the elastic interaction between the two chains along the diagonals, involves the equilibrium distance $D_0(S_{1,i}, S_{2,i\pm1})$ whose expression writes $D_0(S_{1,i}, S_{2,i\pm1}) = \sqrt{\left(R_0^{HH}\right)^2 + [R_0(S_{1,i}, S_{1,i+1})]^2}$ or $\sqrt{\left(R_0^{HH}\right)^2 + [R_0(S_{2,i}, S_{2,i+1})]^2}$, according to the considered diagonal direction.

It is important to notice that, according to Equations (5) and (6), when the chain is totally HS, the equilibrium distance between two nn HS sites is equal to $R_0(+1,+1) = R_0^{HH}$ and that of two nnn HS sites along the chain is systematically equal to $R_0'(+1,+1) = 2R_0^{HH}$, which then satisfies the minimization of the elastic energy. This remark also applies to the LS state. In the following, we will see how can we break this harmony through the presence of an extra strain in the lattice.

2.2. Introduction of the Elastic Frustration

The concept of elastic frustration, which is at the heart of the present paper, assumes the existence of a lattice mismatch between the nn and the nnn equilibrium bond lengths inside the chains. In a previous work [44], we studied the effect of such elastic frustration in an isolated 1D SCO chain by introducing it only between LS-LS and LS-HS neighbors. In the present model, we extend these investigations to two coupled frustrated chains, while keeping, as in the previous study, the HS state free from any elastic frustration, in the two chains.

The idea of elastic frustration consists of the existence of antagonist equilibrium bond lengths between the nn and nnn along the chains when LS-LS and LS-HS configurations are involved. Since no transverse displacement of the sites is allowed in these simulations, once frustrated the system will not be able to totally relax the excess of stress. The new expression of the nn equilibrium bond length, including the frustration effect between sites i and $i+1$ in the two chains, is written as follows:

$$R(S_{\ell,i}, S_{\ell,i+1}) = R_0(S_{\ell,i}, S_{\ell,i+1}) + \frac{\delta_R \xi_\ell}{2}\left(1 - \frac{S_{\ell,i} + S_{\ell,i+1}}{2}\right), \tag{7}$$

where, $R_0(S_{\ell,i}, S_{\ell,i+1})$ is the non-frustrated equilibrium nn bond length distance, whose expression is given in Equation (5), with ξ_ℓ $(\ell = 1, 2)$ representing the rates of frustration strength for the two chains. It is important to notice that the expressions of the equilibrium bond lengths of the nnn sites along the chain are still given by Equation (6).

Thus, according to Equation (7), in the case of three consecutive LLL (LS-LS-LS) sites in chain 1, for example, the equilibrium nn distances are equal to $R(-1,-1) = R_0^{LL} + \delta_R \xi_1$, while the nnn equilibrium distance within the chain, is still given by Equation (6), and is equal to $R' = 2R_0^{LL} \neq 2\left(R_0^{LL} + \delta_R \xi_1\right)$. Since geometrically, $R' = 2R$, a bond length misfit does exist between these two quantities, for the reason that the sites can only move along the x direction. With this frustration which constrains the system, the latter is forced to optimize its total elastic energy by moving the neighboring lattice sites and sharing the excess of elastic energy inside the chain, so that the final mechanical equilibrium will clearly depend on the nn and nnn elastic constants as well as on diagonal the elastic coupling between the chains.

2.3. Model Parameters and Resolution Method

To perform the present simulations, we use in both chains the following values of non-frustrated nn equilibrium bond length distances: $R_0^{LL} = 1.0$ nm, $R_0^{HH} = 1.2$ nm and $R_0^{HL} = 1.1$ nm, leading to the following bond length misfit between the LS and HS phases: $\delta_R = 0.2$ nm. The intra-chain elastic constants have been fixed to $E_0 = 24,000$ K.nm^{-2} = 24 mev.Å^{-2} for the nn interactions along the chains, and to $A_0 = 0.1E_0$ for the nnn elastic interactions within the same chain. The diagonal inter-chains elastic constant is fixed to $A_1 = 0.05E_0$. The used value of the ligand field energy is $\Delta_0 = 450$ K, and that of the degeneracy ratio is, $\ln g = 5$, to which corresponds the molar entropy change, $\Delta S = R \ln g \simeq 41$ J.K.Mol^{-1}, which is in fair agreement with experimental data of calorimetry reported in the literature [24].

The MC simulations are performed on two coupled chains, each of which contains 120 sites. The sites are visited randomly along the MC procedure. The stochastic algorithm is performed as follows: for a site i randomly selected, with spin $S_i = \pm 1$ and position, x_i, a new spin value $S_i' = -S_i$ is set without position change. This spin change is updated, using Metropolis transition rates, and whatever the result of this first process (accepted or rejected spin change), a second MC procedure is applied to the lattice positions by performing slight motions of all nodes (selected randomly) with a random displacement of maximum amplitude, $\delta x = 0.05$ nm, which is much smaller than the smallest equilibrium distance $R_0^{LL} = 1$ nm, between sites. This procedure of the lattice relaxation is repeated 10 times for each spin flip in order to reach the mechanical equilibrium. Afterward, a new site is randomly selected and we repeat the procedure until all lattice nodes are visited for the spin change: we then define such step as the unit of the Monte Carlo step "MCS". In the present simulations, the thermal properties are calculated by changing the temperature by 1K step. At each temperature, we perform 2500 MCS to reach the equilibrium state and we use 2500 other MCS for the statistics. Within this procedure, each site is displaced 2500 times for 1 MCS. So, at each temperature, each spin state and lattice position is updated 6×10^7 times, respectively. We have checked that increasing the simulation time does not affect the final results, which ensures that we reached the stationary state for spin and lattice position variables.

3. Results and Discussions

This section is devoted to the detailed study of the thermodynamic properties of this set of two coupled frustrated chains. To this end, we first determine the thermal dependence of the usual macroscopic order parameters describing the spin transition, which is first the HS fractions, n_{HS_ℓ} ($\ell = 1, 2$) of the two chains 1 and 2, which connect to the corresponding average magnetization $< S >_\ell$ ($\ell = 1, 2$) through Equation (8). Concomitantly, we also calculate the thermal dependence of the average intra-chain ($< d >_\ell$) and diagonal inter-chains ($< d >_{12}$) of the instantaneous bond length distances, given by Equations (9) and (10), respectively. The previous average quantities can be simply expressed as:

$$n_{HS_\ell} = \frac{1 + < S >_\ell}{2}, \tag{8}$$

$$< d >_\ell = \frac{\sum_{i=1}^{N_x} (x_{\ell,i+1} - x_{\ell,i})}{(N_x - 1)}, \tag{9}$$

$$< d >_{12} = \frac{\sum_{i=1}^{N_x} \sqrt{\left(x_{2,i+1} - x_{1,i}\right)^2 + \left(R_0^{HH}\right)^2} + \sqrt{\left(x_{1,i+1} - x_{2,i}\right)^2 + \left(R_0^{HH}\right)^2}}{2(N_x - 1)}, \tag{10}$$

where $\ell = 1, 2$ stands for the chain number, $< S >_\ell = \frac{\sum_{i=1}^{N_x} S_{\ell,i}}{N_x}$ is the average spin value of the ℓ^{th} chain, $(x_{\ell,i+1} - x_{\ell,i})$ is the instantaneous nn distance between nn sites inside chain ℓ and

the quantity $\sqrt{\left(x_{2,i+1}-x_{1,i}\right)^2+\left(R_0^{HH}\right)^2}$ is the instantaneous diagonal distance between site $i+1$ of chain 2 and site i of chain 1. The total HS fraction of the whole system is then given by:

$$n_{HS}=\frac{1}{2}\left(n_{HS_1}+n_{HS_2}\right), \tag{11}$$

In view of the complex structure of Hamiltonian (1), the latter is solved numerically by Monte Carlo (MC) technique running on spins S_i and position variables, x_i. Here, we aim to study the thermal properties of this system, considering the frustration rates of the two chains, ξ_1 and ξ_2, as control parameters.

In all the investigations outlined below, we start the simulations from the high-temperature phase, where the lattice is prepared in the HS phase, by fixing all spins to $S_i=+1$ and all nn (resp. nnn) bond length distances equal to R_0^{HH} (resp. $2R_0^{HH}$). The advantage is that this state is not frustrated by construction, and therefore the total elastic energy of the initial lattice is null.

3.1. Frustration of the First Chain

In the first step, we impose an elastic frustration in the nn equilibrium bond lengths solely in the first chain, and we let the second without frustration, which means that we fix $\xi_2=0$. Our objective here is to investigate the effect of the frustration of the first chain 1 on the thermal properties of chain 2 while monitoring the frustration parameter ξ_1, with values ranging from 0 to 1.3.

3.1.1. Thermal Dependence of the HS Fraction

The obtained results are summarized in Figure 2, where the panel of Figure 2a displays the thermal dependence of the HS fraction, n_{HS1}, of chain 1 for different values of ξ_1. In the absence of frustration ($\xi_1=0$), one obtains a hysteretic first-order transition of width $\Delta T=8.4$ K. This result may be found quite surprising for a 1D chain. However, the volume (here the length) change, accompanying that of the spin state, generates infinite long-range interactions between the spin states, leading the system to belong to the mean-field universality class, as demonstrated by several authors [48] even at 3D [46,49]. This important property allows obtaining long-lived metastable states around the transition temperatures on heating and cooling, at the origin of the hysteretic character of these first-order transitions.

When elastic frustration comes into play (i.e., $\xi_1\neq 0$ in Figure 2a), the curve of the thermal dependence of the HS fraction of chain 1 shifts to the low-temperature region, and the transition transforms from first-order with hysteresis to a continuous two-step transformation with a large plateau around $n_{HS1}=0.5$. In the panel of Figure 2b, is presented the corresponding thermal dependence of the HS fraction, n_{HS2}, of chain 2. It is remarked that in the absence of frustration in chain 1, chain 2 displays exactly the same curve of HS fraction as that of chain 1. This is well understood when examining Hamiltonians (2) and (3) which are equivalent for $\xi_1=\xi_2$. In contrast, when chain 1 is frustrated, a symmetry breaking occurs between the two Hamiltonians, since exchanging the indexes 1 by 2 and vice versa does not keep the total Hamiltonian invariant. Consequently, the two chains are expected to have different behaviors. Indeed, the comparison between Figure 2a,b clearly shows that chain 2 (Figure 2b) feels a strong elastic strain that deforms its HS fraction curve by decreasing the transition temperature. Beyond the value $\xi_1=0.3$, the previous mechanism is accompanied by the appearance of humps along the thermal transition, for small HS fractions values, announcing the existence of a slight two-step transition. Interestingly, above some threshold value of ξ_1, located in the interval 0.6–0.8, chain 2 experiences incomplete spin transitions, characterized by the presence of a residual HS fraction at low temperature, whose amplitude increases with the frustration rate ξ_1 of chain 1.

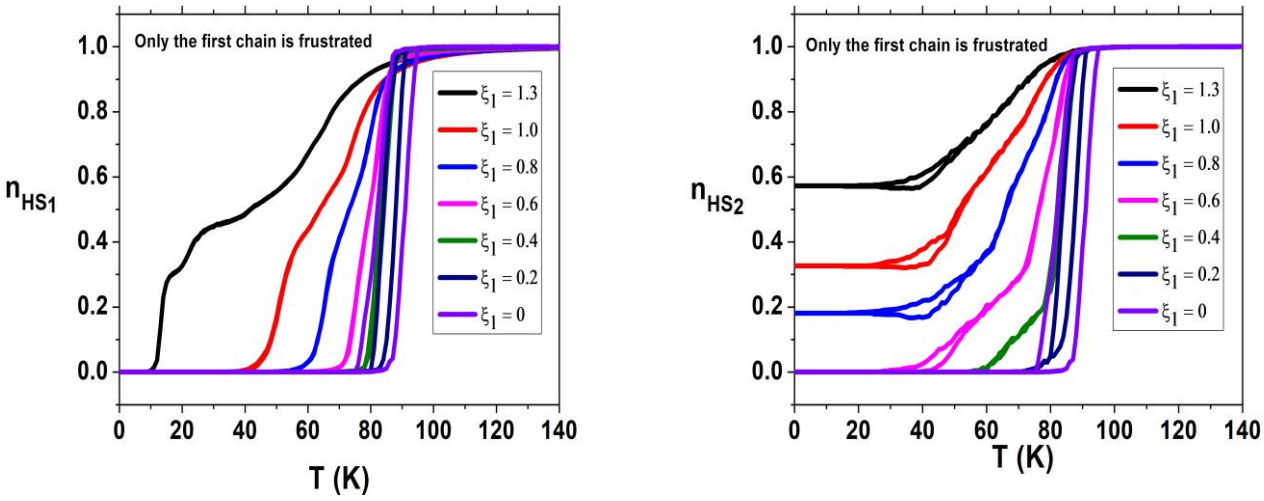

Figure 2. (**a**) Thermal dependence of the HS fraction n_{HS1} of chain 1 for different values of the elastic frustration rate, ξ_1, showing the occurrence of discontinuous and hysteretic first-order transitions for $\xi_1 < 0.6$ and continuous multi-step transitions for higher ξ_1 values. (**b**) Corresponding thermal dependence of the HS fraction n_{HS2} of chain 2, showing a similar behavior with the presence at a low temperature of a residual HS fraction beyond $\xi_1 > 0.6$.

We have studied the ξ_1-dependence of this residual HS fraction emerging in chain 2, noted n^*_{HS2}, the behavior of which is summarized in Figure 3. The results clearly indicate the existence of a critical value $\xi_C \cong 0.6$, beyond which the LS state is no more the stable state at 0K in chain 2, while chain 1 which directly experiences the elastic frustration, is already in the LS phase. Remarkably, Figure 3 indicates that beyond ξ_C the residual fraction, n^*_{HS2}, linearly increases with the frustration rate ξ_1.

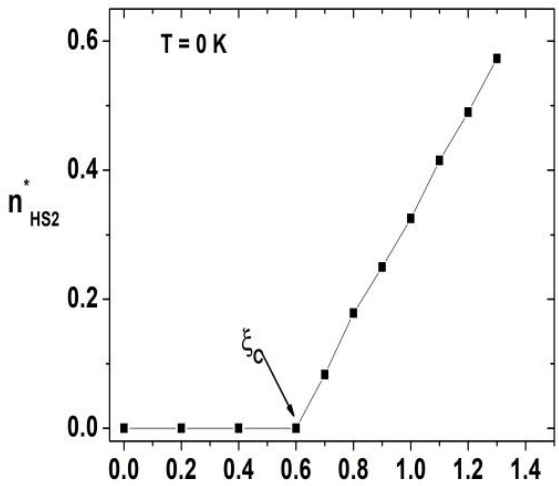

Figure 3. Low temperature (0 K), frustration rate ξ_1-dependence of the residual HS fraction, n^*_{HS2}, of chain 2, derived from Figure 2b. Notice the existence of a threshold value $\xi_C \cong 0.6$ above which n^*_{HS2} linearly increases with ξ_1.

3.1.2. Thermal Dependence of the Lattice Bond Lengths

To understand the origin of the two-step (resp. incomplete) transitions appearing in chain 1 (resp. 2) of Figure 2b above the threshold value, $\xi_1 = \xi_C = 0.6$, we plot in Figure 4a–c the corresponding thermal behaviors of the average nn lattice intra-chains bond lengths $< d >_1$ (Figure 4a), $< d >_2$ (Figure 4b), and interchain distance, $< d >_{12}$ (Figure 4c).

It is immediately remarked that as soon as ξ_1 is nonzero, the average low-temperature bond lengths $< d >_1$, $< d >_2$, and $< d >_{12}$ become larger than their expected equilibrium LS values, which are, respectively, 1.0, 1.0 and $\sqrt{2.44}$ nm.

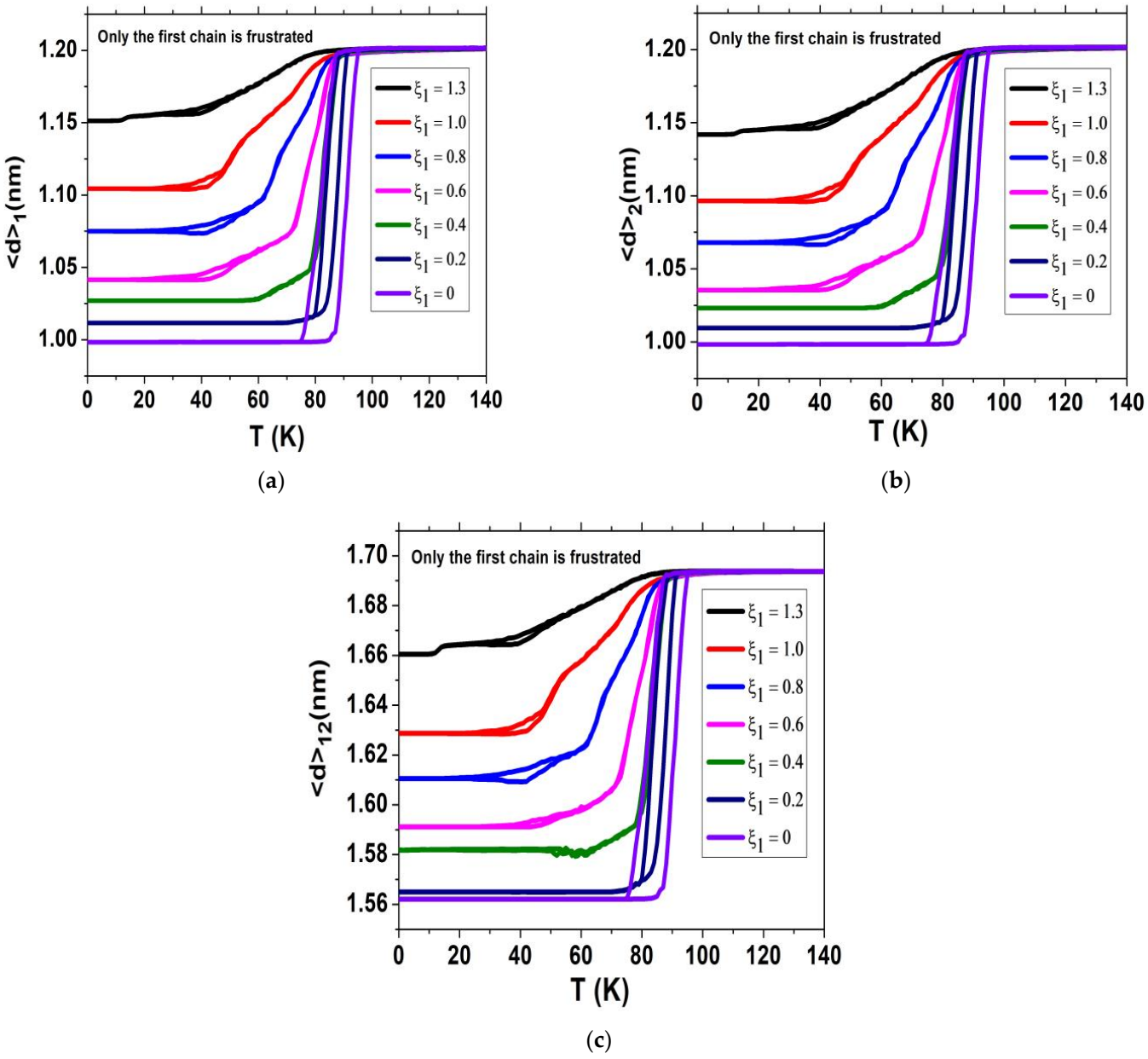

Figure 4. Thermal dependences of the average nn distances, $< d >_1$ of chain 1 (**a**), $< d >_2$ of chain 2 (**b**) and $< d >_{12}$ along the diagonal interchain direction (**c**). The data correspond to those of Figure 2. All figures show a monotonous increase in the relaxed lattice parameter of the LS state (i.e., $< r_{ij} >$ at 0 K) as ξ_1 increases.

The analysis of the results of Figures 3 and 4 and the correlation of the electronic and the elastic properties of the lattice, lead to the conclusion that when $< d >_1$ exceeds the value $< d >_1 = R^{HL} = 1.1$ nm (see black curve in Figure 4a) for $\xi_1 = 1.0$, a plateau starts to emerge in the thermal dependence of n_{HS1} in Figure 2a and concomitantly a nonzero residual HS fraction appears in the 2nd chain (Figure 2b). This proves, once more, that chain 2 (Figure 4b) follows the same behavior as that of chain 1, although the values of the average parameter $< d >_2$ differ slightly from those of $< d >_1$ when the frustration rate ξ_1 increases, due to the interchain elastic coupling. In Figure 4c, the diagonal bond length

$< d >_{12}$ between the two chains also follows the same trends with temperature as $< d >_1$ and $< d >_2$, except for the behavior of $< d >_{12}$ at 0 K which presents a few differences from those of $< d >_1$ and $< d >_2$.

Overall, ξ_1 induces a negative internal pressure in the lattice resulting in tensile stress. According to Figure 4a,b, the latter is bigger for chain 1 than for chain 2, as clearly confirmed by the data of Figure 5a, where we plotted the 0 K values of $< d >_1$ and $< d >_2$ as function of ξ_1. In addition, the difference $(< d >_1 - < d >_2)$ even increases as a function of ξ_1 (Figure 5b). However, contrary to the thermal behaviors of the HS fractions of the two chains, given in Figure 2a,b, the corresponding average nn bond lengths $< d >_1$ and $< d >_2$ show very similar temperature dependence trends, as demonstrated by Figure 5c, which illustrates an almost perfect linear correlation between these two parameters.

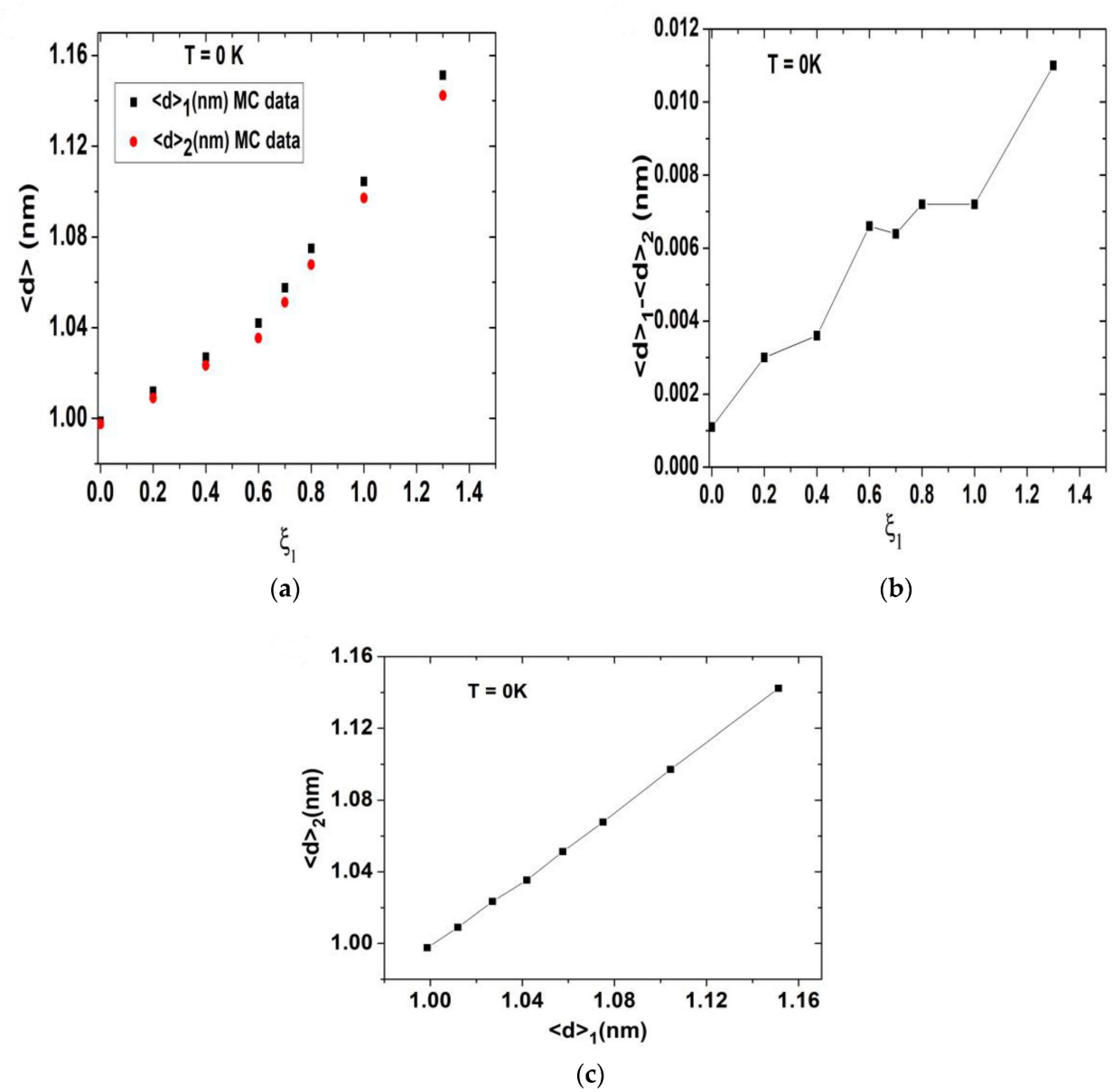

Figure 5. (**a**) Relaxed 0 K nn distances, $< d >_1$, $< d >_2$ in panel (**a**) and $(< d >_1 - < d >_2)$ in panel (**b**) in the LS state vs. the frustration rate, ξ_1. Panel (**c**) depicts a remarkable linear behavior of $< d >_2$ vs. $< d >_1$, indicating a fair correlation between these two parameters.

To summarize this part, it is important to keep in mind that the elastic frustration is only injected in chain 1. As a result, in the LS state, for example, all equilibrium distances of chain 1 become bigger than those of LS, which forces chain 1 to expand. However, since

the latter is coupled to chain 2 by imposing all nn interchain distances as invariant (see Figure 1), this constraint enhances the frustration in both chains. Therefore, the intermediate plateaus obtained in chain 2 are caused by the behavior of the first chain which experiences a stronger elastic frustration, the part of which is transferred to chain 2, via the diagonal interchain interactions.

3.1.3. Self-Organization of the Spin States and Lattice Bond Lengths

To provide more insights into the electronic organization mode inside the plateau region, we plot in Figure 6, the spatial configurations of the spin states (red dots = HS and blue dots = LS) inside the lattice along the two-step thermal transitions (see Figure 2a) of chain 1, for the frustration rate value, $\xi_1 = 1.3$. An undeniable evidence of the occurrence of an ordered LLHHLL ... state, noted for simplicity L2H2, is identified in the plateau region in the interval $25 \leq T \leq 40$ K. In the same Figure 6, we depict the corresponding spatial configurations of the spin states along the thermal transition of chain 2 (black curve of Figure 2b), which is characterized by the emergence of a residual fraction $n_{HS2} \sim \frac{2}{3}$ at low temperature, where an ordered state LLHHHH ... , noted for simplicity L2H4 is also evidenced. In addition, it is important to notice for both self-organized states, the presence of antiphase boundaries, since the symmetric configurations, H2L2 (resp. H4L2) have the same energies as L2H2 (resp. L2H4).

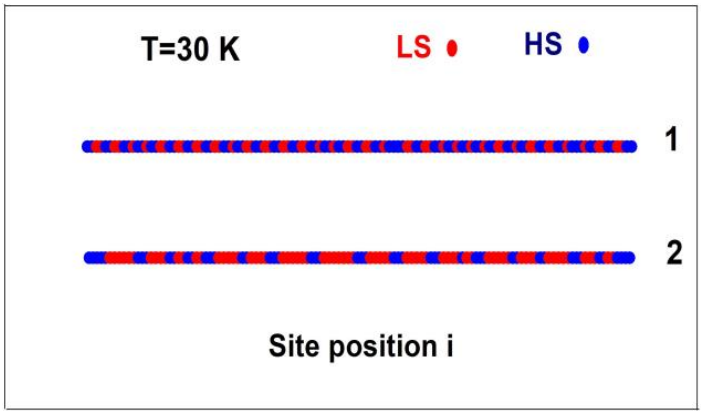

Figure 6. Snapshots of the spatial distribution of the spin states of the two chains at $T = 30$ K and for $\xi_1 = 1.3$, corresponding to the plateau region of the black curves of Figure 2a,b. Chain 1 (Figure 2a) shows an antiferromagnetic-like organization of type L2H2, while chain 2 displays an antiferromagnetic-like organization of type L2H4 (Figure 2b).

Interestingly, this self-organization of the spin states is accompanied by that of the nn bond lengths along the two chains. To check this aspect, we draw in Figure 7a the behavior of the interatomic distance, $d_x = x_{i+1} - x_i$, along chain 1, corresponding to the self-organization of Figure 6. A clear periodic modulation of the lattice bond length is identified, showing the existence of a quasi-periodic oscillating sequence of d^{HH}, d^{HL}, d^{LL} distances, perturbed at some points by the presence of the antiphase boundaries, in excellent agreement with the predicted H2L2 structure of Figure 6. Similarly, the dependence of nn bond length $d_x = x_{i+1} - x_i$ along the x-direction for the chain 2 (Figure 7b) also gives a periodic modulated structure, which is consistent with the L2H4 self-organized spin state of Figure 6, since now the nn distances follow the periodic sequence, d^{HH}, d^{HH}, d^{HH}, d^{HL}, d^{LL}.

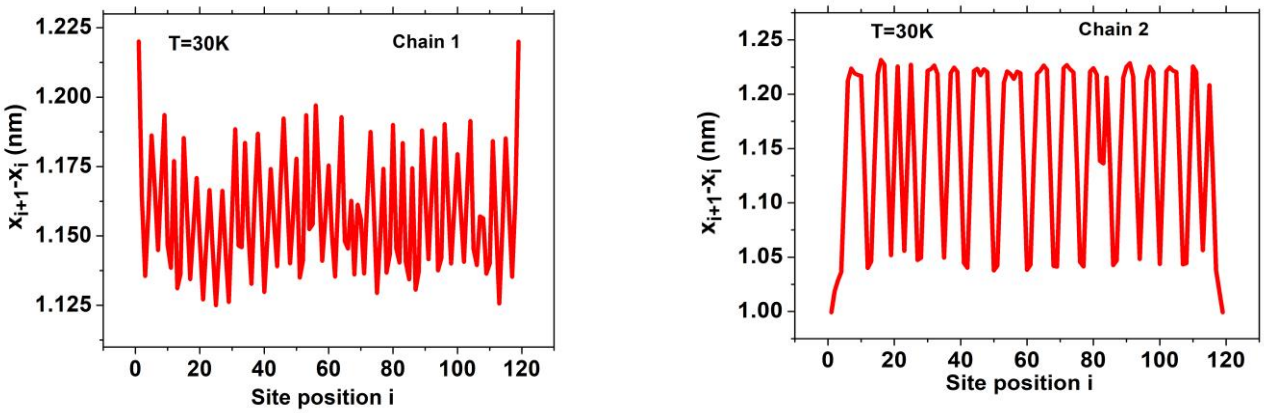

(**a**) (**b**)

Figure 7. Space-dependence of the nn bond length, in the plateau region corresponding to the snapshot of Figure 6, (**a**) along chain 1 showing a spatial modulation, corresponding to a perfect L2H2 structure and (**b**) along chain 2, denoting a periodic spin state organization of type L2H4. The model parameters are the same as those of Figure 4, except for $\xi_1 = 1.3$ and $T = 30$ K.

3.2. Both Chains Are Frustrated

Now we study the general situation where both chains are frustrated according to Equation (7), with respective frustration rates, ξ_1 and ξ_2, in such a way as to cause antagonist distances between nn and nnn sites. Our objective here is to investigate the thermal behavior of each chain subsystem as a function of the values of the frustrations ξ_1 and ξ_2 in order to investigate their mechanical interplay through the analysis of their nn intra- and nnn interchain interactions. In these calculations, we fix $\xi_1 = 1.3$ and we vary ξ_2 in the interval 0 to 1.1.

3.2.1. Thermal Dependence of the HS Fraction

The results of the MC simulations are summarized in Figure 8, where we report the thermal behaviors of the HS fractions of each chain for various ξ_2 values. In Figure 8a, we recall for comparison the case already presented in Figure 2a of $\xi_1 = 1.3$ and $\xi_2 = 0$ (black curve), which results in the occurrence of a double-step transition with a plateau around $n_{HS1} = 0.5$ for chain 1, and an incomplete spin transition with a residual HS fraction, $n^*_{HS2} \simeq \frac{2}{3}$ at low temperature in chain 2. When the frustration of chain 2 comes into play, the value of its residual HS fraction, n^*_{HS2}, decreases gradually to 0.38 for $\xi_2 = 0.2$ (Figure 8b) to reach finally $n^*_{HS2} = 0$ (LS) for $\xi_2 = 0.4$ (Figure 8c). This transformation is accompanied by the emergence of a first plateau around $n_{HS} = 0.5$ in the total HS fraction (blue curve in Figure 8c). When ξ_2 exceeds the value 0.6 (see Figure 8d), a second plateau starts to appear in the thermal dependence of the total HS fraction n_{HS} around $n_{HS} = 0.25$ (see Figure 8e). For higher frustration values, the thermal dependence of the HS fraction exhibits three steps (Figure 8f–h) and even four-step spin transitions for $\xi_2 = 1.1$ (Figure 8g), with the presence of several plateaus in the total HS fraction (blue curve in Figure 8g). For $\xi_1 = \xi_2 = 1.3$, the two chains become equivalent and the thermal dependences of their HS fractions perfectly overlap, as seen in Figure 8h.

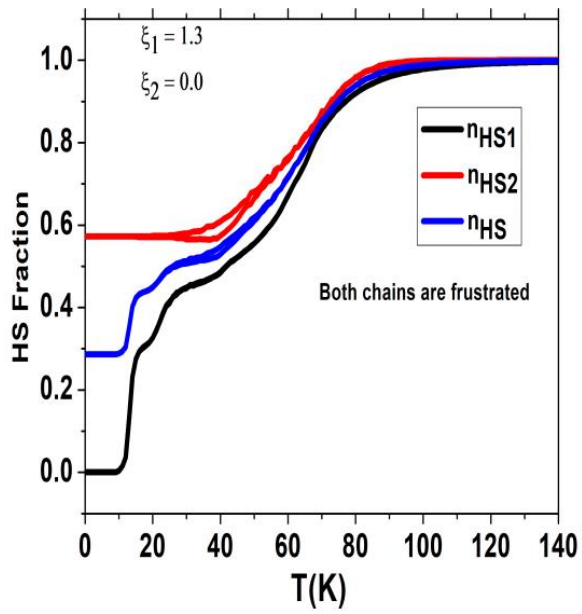

(**a**)

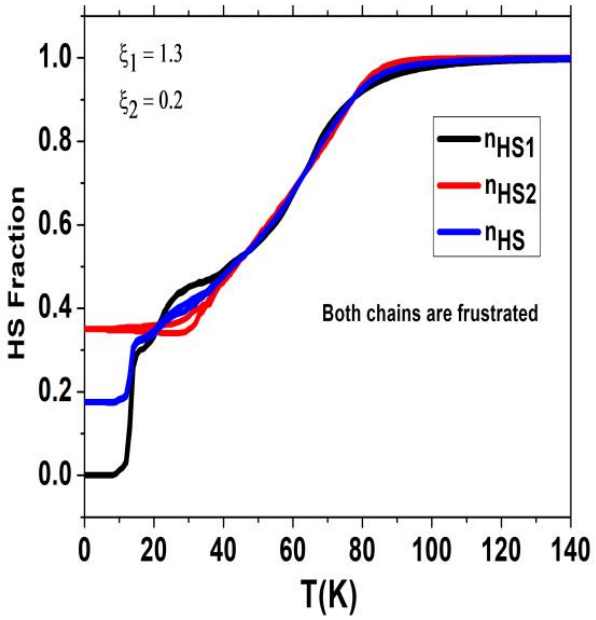

(**b**)

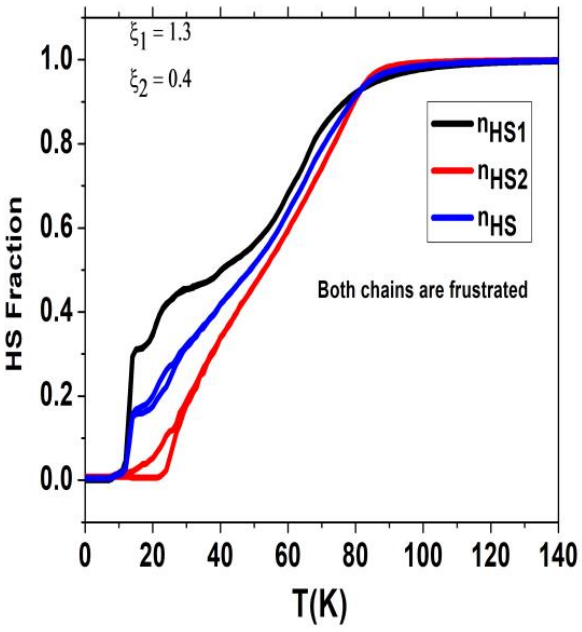

(**c**)

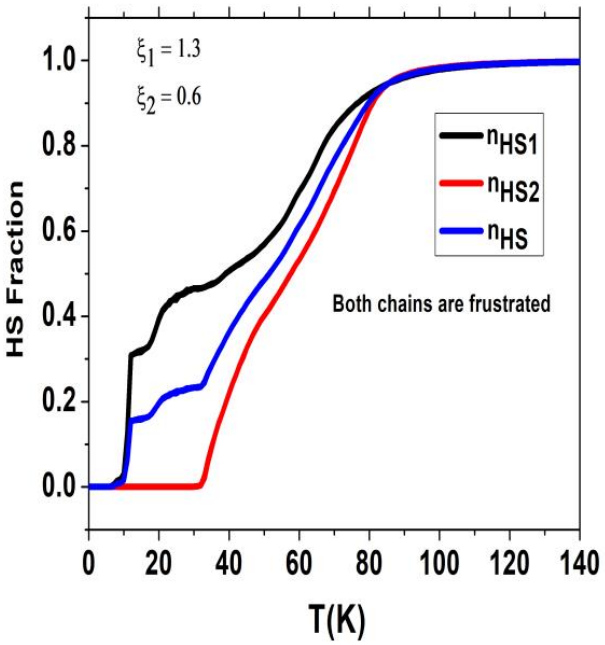

(**d**)

Figure 8. *Cont*.

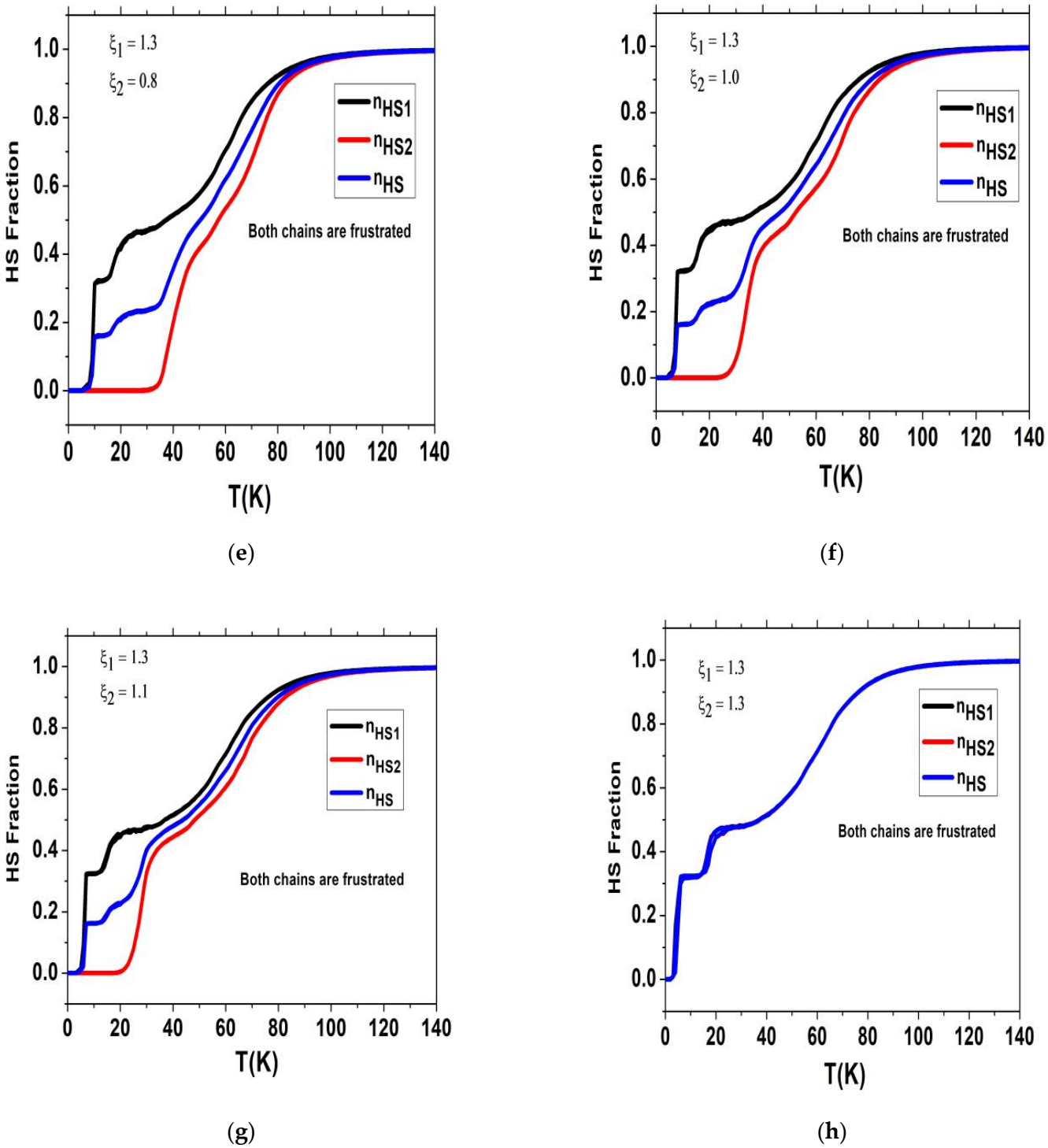

Figure 8. MC results of the thermal dependence of the HS fraction, n_{HS1}, of chain 1, n_{HS2}, of chain 2 and that of the average HS fraction n_{HS}, of Hamiltonian (1) for different values of the elastic frustrations strengths, ξ_1, and ξ_2, showing the occurrence of multi-step transitions. ξ_1 is fixed to 1.3 in all figures. From panel (**a**–**h**), $\xi_2 = 0$, 0.2, 0.4, 0.6, 0.8, 1.0, 1.1, and 1.3, respectively.

3.2.2. Self-Organization of the Spin States in the Plateau Regions

To obtain a clearer view of the organization mode of the spin states inside the plateau regions of Figure 8, we plot in Figure 9 the spatial configurations of the spin states (red dots = HS and blue dots = LS), for both chains (identified by 1 and 2 in the figures) along

the thermal transition of the three-step behavior of Figure 8g, for three temperature values, $T = 37$, 18, and 10 K.

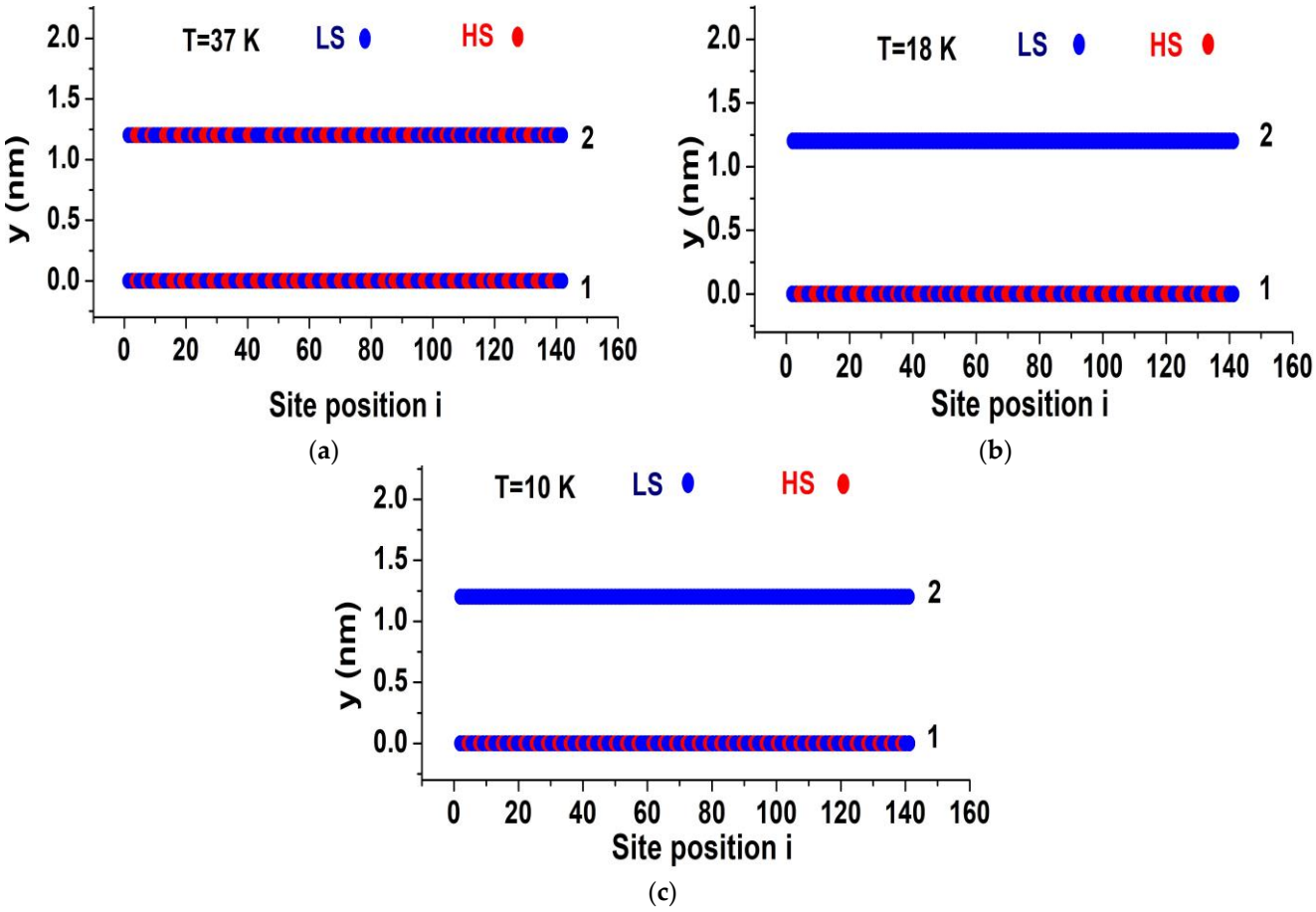

Figure 9. Selected snapshots of the spatial distribution of the spin states of two coupled SCO chains of 120 sites, corresponding to Figure 8g. An antiferromagnetic-like organization in the plateau regions of the black and red curves of Figure 8g is obtained for (**a**) $T = 37$ K, (**b**) $T = 18$ K, and (**c**) $T = 10$ K. The model parameters are the same as those of Figure 8g, where $\xi_1 = 1.3$ and $\xi_2 = 1.1$.

The first snapshot, presented in Figure 9a, associated with the highest plateau of Figure 8g, at T = 37 K and $n_{HS} \cong 0.5$, depicts the presence of a special antiferromagnetic-like structure, made of dimerized LL-HH-LL-HH spin states along the two chains. This structure is perfectly consistent with the previous HS fraction value. In contrast, it is clearly different from the usual antiferromagnetic-like HLHLHL structures, usually reported in the literature of 2D Ising-like models, except for the case of frustrated nnn Ising-like model combining competing nearest and next-nearest exchange-like interactions [35,36], which are introduced by hand to produce the sought-after effect.

The second snapshot, presented in Figure 9b, shows a mixture of antiferromagnetic-like structures, L2H2 and H2L configurations, emerging in chain 1 at $T = 18$ K, while chain 2 is fully LS, leading to an average HS total fraction equal to $\frac{1}{6}$, in agreement with the data of Figure 8g. In the third snapshot, reported in Figure 9c, and obtained at 10 K, chain 1 self-organizes with the special structure LH2LH2 . . . , displaying a periodic alternation of antiferro and ferro short-range ordering, while chain 2 is fully LS, a situation which is also consistent with the results of Figure 8g.

Let us come back now to the panel of Figure 9a. Here, the meticulous inspection of the interchain ordering indicates that the two chains are clearly antiferro-elastically coupled. However, the presence of antiphase boundaries induces some disorder due to the energetic equivalence of the LL-HH-LL... and the HH-LL-HH configurations. To confirm

the emergence of this interchain antiferro-elastic coupling, we present in Figure 10 the spatial dependence along x-direction of the spin products $S_{i,1} \times S_{i,2}$ of two sites of the same rank i, belonging to different chains for the temperature $T = 37$ K. The behavior of $S_{i,1} \times S_{i,2}$ as function of i clearly confirms the presence of an antiferro-like organization ($S_{i,1} \times S_{i,2} = -1$) between the two chains in the intervals $5 \leq i \leq 35$, $82 \leq i \leq 90$ and $110 \leq i \leq 120$ while ferromagnetic-like organizations ($S_{i,1} \times S_{i,2} = +1$) are obtained for $35 \leq i \leq 80$ and $90 \leq i \leq 110$.

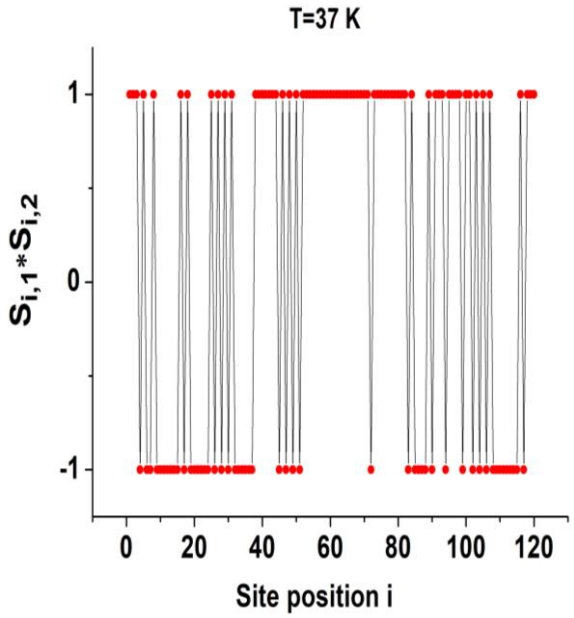

Figure 10. The product $S_{i,1} \times S_{i,2}$ as a function of the site positions of two coupled chains of 120 sites, corresponding to Figure 8g at $T = 37$ K. Notice the clear coexistence of alternate ferromagnetic ($S_{i,1} \times S_{i,2} = +1$) and antiferromagnetic-like ($S_{i,1} \times S_{i,2} = -1$) inter-chains orders. The model parameters are the same as those of Figure 8g, where for $\xi_1 = 1.3$ and $\xi_2 = 1.1$.

4. Conclusions

One-dimensional spin crossover solids are widely studied in the literature due to their specific anisotropic character which allows many original behaviors, such as large thermal hysteresis, incomplete as well as multi-step spin transitions. Therefore, they represent excellent objects of study for theoreticians due to their one-dimensional character, which presupposes a simple implementation and rapid calculations when they are modeled. In previous works [42,43], we have analyzed the origin of multi-step transitions in an isolated 1D binuclear SCO chain, by adapting the original electro-elastic model in which we introduced an elastic frustration in the intra-binuclear bond length distances. In the present work, we have extended our model to investigate the thermal behaviors of an SCO system made of two elastically coupled mononuclear chains. Each chain contains N SCO sites that are coupled through springs with their nearest and next-nearest neighbors. The elastic interchain interactions include diagonal springs, while the nn inter-chain distance is assumed as invariant. As a result, the atoms in both chains can only move along the longitudinal directions, which then imposes a strong constraint or a geometrical frustration during the expansion and the contraction of the chains, corresponding respectively to transitions into the HS and LS states. In addition, specific frustrations, related to the existence of antagonist nn and nnn distances are injected in the chains. In the end, the model is solved using Monte Carlo simulations, performed on the spin states and the lattice positions. The obtained results can be summarized as follows. First, when we frustrate only the nn bond lengths of the first chain, with an elastic frustration strength ξ_1, we demonstrate that the thermal dependence of the HS fraction curve of the second chain strongly deforms by decreasing its transition temperature. The latter effect is accompanied

by the emergence of a significant residual HS fraction at low temperatures, whose amount linearly increases with the rate of frustration, ξ_1. The interplay between the two chains is attributed to the role of the elastic strength generated by the elastic interchain interaction along the diagonal directions.

In the second step, we frustrated both chains by imposing different frustration rates, ξ_1 and ξ_2. We found that, for higher frustration values in the two chains, the thermal dependence of the HS fraction of each chain exhibits three and even four plateaus upon HS to LS transitions. Moreover, the analysis of the spatial organization of the spin states in these intermediate states revealed the existence of several unexpected and complex configurations in the case of strong and different elastic frustration rates in the two chains. These results also significantly depend on temperature. Thus, while for $\xi_1 = \xi_2$ the two chains are equivalent, an important difference takes place for $\xi_1 \neq \xi_2$. Indeed, in this particular case, new types of self-organizations of the spin states are obtained, such as HH-LL-HH-LL ... for chain 1 and LL-HH-LL-HH ... for chain 2. This type of spatial modulation of the spin state, which is also accompanied by a spatial organization of the lattice bond lengths, is interesting and opens the way for a new type of self-organization of the spin states for systems with a higher number of chains.

On the basis of the findings presented here, the extension of the current model to investigate the effect of the frustration on the dynamics of the LS to HS photo-excitation mechanism through LIESST [50–52] (Light-Induced Spin State Trapping) might be very instructive. Moreover, the analysis of isothermal relaxation of the metastable photo-induced HS state, searching for evidence of multi-step relaxation processes, reminiscent of the thermal behavior of the system, deserves to be considered in the near future. Finally, it is interesting to highlight that all developed ideas related to the effect of elastic frustration and lattice anisotropy can be easily extended to Fe-Co Prussian blue analogs (PBA) [53,54] and valence tautomeric (VT) systems [55–58] which have very similar elasticity and bistability characteristics as SCO materials. In the case of PBA (resp. VT) the spin transition of Co is accompanied by a charge transfer between Co and Fe (resp. ligand) with a significant change in volume. Thus, the same ingredients as those of SCO exist also for these families of charge transfer solids.

Author Contributions: Conceptualization, K.B.; methodology, K.B.; software, K.B., R.T. and H.O.; writing—original draft preparation, K.B. and R.T.; editing, K.B., R.T. and H.O.; funding acquisition, K.B. All authors have read and agreed to the published version of the manuscript.

Funding: This research was funded by ANR (Agence Nationale de la Recherche Scientifique), grant number Mol-CoSM No. ANR-20-CE07-0028-02 and the Universities of Versailles and Paris-Saclay-UPSAY, the CNRS (Centre National de la Recherche Scientifique) and LIA (International Associate French Japan Laboratory). We thank all of them for their financial support.

Data Availability Statement: The data of this manuscript are available within the manuscript.

Acknowledgments: This project has received financial support from the CNRS through the MITI interdisciplinary programs through its exploratory research program, as well as from the ANR project Mol-CoSM No. ANR-20-CE07-0028-02, the Universities of Versailles and Paris-Saclay-UPSAY. We thank all of them for their strong support.

Conflicts of Interest: The authors declare no competing financial interests.

References

1. Phan, H.; Benjamin, S.M.; Steven, E.; Brooks, J.S.; Shatruk, M. Photomagnetic Response in Highly Conductive Iron(II) Spin Crossover Complexes with TCNQ Radicals. *Angew. Chem. Int. Ed.* **2015**, *54*, 823. [CrossRef]
2. Ohkoshi, S.I.; Tokoro, H. Photomagnetism in Cyano-Bridged Bimetal Assemblies. *Acc. Chem. Res.* **2012**, *45*, 1749. [CrossRef]
3. Coronado, E.; Galán-Mascarós, J.R.; Monrabal-Capilla, M.; García-Martínez, J.; Pardo-Ibáñez, P. Bistable Spin-Crossover Nanoparticles Showing Magnetic Thermal Hysteresis near Room Temperature. *Adv. Mater.* **2007**, *19*, 1359. [CrossRef]
4. Kahn, O.; Jay-Martinez, C. Spin-Transition Polymers: From Molecular Materials. *Towar. Mem. Devices Sci.* **1998**, *279*, 44.
5. Gütlich, P.; Hauser, A.; Spiering, H. Thermal and Optical Switching of Iron(II) Complexes. *Angew. Chem. Int. Ed.* **1994**, *33*, 2024–2054. [CrossRef]

6. Gütlich, P.; Goodwin, H.A. *Spin Crossover in Transition Metal Compounds Iron(II)*; Springer: Berlin/Heidelberg, Germany, 2004; Volume 233, pp. 234–235.
7. Olguín, J.; Brooker, S. Spin Crossover Active Iron(II) Complexes of Selected Pyrazole-Pyridine/Pyrazine Ligands. *Coord. Chem. Rev.* **2011**, *255*, 203–240. [CrossRef]
8. Gütlich, P.; Gaspar, A.B.; Garcia, Y. Spin State Switching in Iron Coordination Compounds. *Beilstein. J. Org. Chem.* **2013**, *9*, 342–391. [CrossRef] [PubMed]
9. Li, Z.Y.; Dai, J.W.; Shiota, Y.; Yoshizawa, K.; Kanegawa, S.; Sato, O. Multi-Step Spin Crossover Accompanied by Symmetry Breaking in an Fe(III) Complex: Crystallographic Evidence and DFT Studies. *Chem. Eur. J.* **2013**, *19*, 12948–12952. [CrossRef] [PubMed]
10. Jureschi, C.M.; Linares, J.; Rotaru, A.; Ritti, M.H.; Parlier, M.; Dîrtu, M.M.; Wolff, M.; Garcia, Y. Pressure Sensor via Optical Detection Based on a 1D Spin Transition Coordination Polymer. *Sensors* **2015**, *15*, 2388–2398. [CrossRef]
11. Decurtins, S.; Gütlich, P.; Hasselbach, K.M.; Hauser, A.; Spiering, H. Light-induced excited-spin-state trapping in Iron(II) spin-crossover systems. Optical spectroscopic and magnetic susceptibility study. *Inorg. Chem.* **1985**, *24*, 2174–2178. [CrossRef]
12. Hauser, A. Reversibility of light-induced excited spin state trapping in the $Fe(ptz)_6(BF4)_2$, and the $Zn_{1-x}Fe_x(ptz)_6(BF4)_2$ spin-crossover systems. *Chem. Phys. Lett.* **1986**, *124*, 543–548. [CrossRef]
13. Hauser, A.; Adler, J.; Gütlich, P. Light-induced excited spin state trapping (LIESST) in [$Fe(2\text{-mephen})^3]^{+2}$ embedded in polymer matrices. *Chem. Phys. Lett.* **1988**, *152*, 468–472. [CrossRef]
14. Gütlich, P.; Garcia, Y.; Goodwin, H.A. Spin crossover phenomena in Fe(II) complexes. *Chem. Soc. Rev.* **2000**, *29*, 419–427. [CrossRef]
15. Hauser, A. Light-Induced Spin Crossover and the High-Spin Low-Spin Relaxation. In *Spin Crossover in Transition Metal Compounds*; Topics in Current Chemistry; Springer: New York, NY, USA, 2004; Volume 234, pp. 155–198.
16. Mahfoud, T.; Molnar, G.; Bonhommeau, S.; Cobo, S.; Salmon, L.; Demont, P.; Tokoro, H.; Ohkoshi, S.; Boukheddaden, K.; Bousseksou, A. Electric-Field-Induced Charge-Transfer Phase Transition: A Promising Approach Toward Electrically Switchable Devices. *J. Am. Chem. Soc.* **2009**, *131*, 15049–15054. [CrossRef]
17. Rotaru, A.; Dugay, J.; Tan, R.P.; Guralskiy, I.A.; Salmon, L.; Demont, P.; Carrey, J.; Molnar, G.; Respaud, M.; Bousseksou, A. Nanoelectromanipulation of Spin Crossover Nanorods: Towards Switchable Nanoelectronic. *Devices Adv. Mater.* **2013**, *25*, 1745–1749. [CrossRef]
18. Prins, F.; Monrabal-Capilla, M.; Osorio, E.A.; Coronado, E.; van der Zant, H.S. Room-Temperature Electrical Addressing of a Bistable Spin-Crossover Molecular System. *Adv. Mater.* **2011**, *23*, 1545–1549. [CrossRef]
19. Slimani, A.; Boukheddaden, K.; Varret, F.; Oubouchou, H.; Nishino, M.; Miyashita, S. Microscopic spin-distortion model for switchable molecular solids: Spatiotemporal study of the deformation field and local stress at the thermal spin transition. *Phys. Rev. B* **2013**, *87*, 014111. [CrossRef]
20. Moussa, N.O.; Ostrovskii, D.; Garcia, V.M.; Molnár, G.; Tanaka, K.; Gaspar, A.B.; Real, J.A.; Bousseksou, A. Bidirectional photoswitching of the spin state of iron(II) ions in a triazol based spin crossover complex within the thermal hysteresis loop. *Chem. Phys. Lett.* **2009**, *477*, 156–159. [CrossRef]
21. Shepherd, H.J.; Rosa, P.; Fallis, I.A.; Guionneau, P.; Howard, J.A.K.; Goeta, A.E. Structural origin of the gradual spin transition in a mononuclear iron(II) complex. *Phys. Chem. Solids* **2012**, *73*, 193–197. [CrossRef]
22. Takahashi, K.; Mori, H.; Kobayashi, H.; Sato, O. Mechanism of reversible spin transition with a thermal hysteresis loop in [FeIII(qsal)2][Ni(dmise)2] · 2CH3CN: Selenium analogue of the precursor of an Fe(III) spin-crossover molecular conducting system. *Polyhedron* **2009**, *28*, 1776. [CrossRef]
23. Fedaoui, D.; Bouhadja, Y.; Kaiba, K.; Guionneau, P.; Létard, J. Complexation of 2,6-Bis(3-pyrazolyl)pyridine–Bis(thiocyanato)iron(II) with a Bridging 4,40-Bipyridine: A New Example of a Dinuclear Spin Crossover Complex. *Eur. J. Inorg. Chem.* **2008**, *7*, 1022–1023. [CrossRef]
24. De Gaetano, Y.; Jeanneau, E.; Verat, A.Y.; Rechignat, L.; Bousseksou, A.; Matouzenko, G.S. Ligand-Induced Distortions and Magneto-Structural Correlations in a Family of Dinuclear Spin Crossover Compounds with Bipyridyl-Like Bridging Ligands. *Eur. J. Inorg. Chem.* **2013**, *2013*, 1015–1023. [CrossRef]
25. Sciortino, N.F.; Scherl-Gruenwald, K.R.; Chastanet, G.; Halder, G.J.; Chapman, K.W.; Létard, J.F.; Kepert, C.J. Hysteretic Three-Step Spin Crossover in a Thermo-and Photochromic 3D Pillared Hofmann-type Metal–Organic Framework. *Angew. Chem. Int. Ed. Engl.* **2012**, *124*, 10301–10305. [CrossRef]
26. Romstedt, H.; Spiering, H.; Gütlich, P. Modelling of two step high spinlow spin transitions using the cluster variation method. *J. Phys. Chem. Solids* **1998**, *59*, 1353–1362. [CrossRef]
27. Piñeiro-López, L.; Valverde-Muñoz, F.J.; Trzop, E.; Muñoz, M.C.; Seredyuk, M.; Castells-Gil, J.; da Silva, I.; Martí-Gastaldo, C.; Collet, E.; Real, J.A. Guest induced reversible on-off switching of elastic frustration in a 3D spin crossover coordination polymer with room temperature hysteretic behaviour. *Chem. Sci.* **2020**, *12*, 1317–1326. [CrossRef]
28. Watanabe, H.; Tanaka, k.; Bréfuel, N.; Cailleau, H.; Létard, J.-F.; Ravy, S.; Fertey, P.; Nishino, M.; Miyashita, S.; Collet, E. Ordering phenomena of high-spin/low-spin states in stepwise spin-crossover materials described by the ANNNI model. *Phys. Rev. B* **2016**, *93*, 014419. [CrossRef]
29. Pittala, N.; Cuza, E.; Pinkowicz, D.; Magott, M.; Marchivie, M.; Boukheddaden, K.; Triki, S. Antagonist elastic interactions tuning spin crossover and LIESST behaviours in FeII trinuclear-based one-dimensional chains. *Inorg. Chem. Front.* **2022**, *9*, 6468–6481. [CrossRef]

30. Ndiaye, M.; Yogendra, S.; Fourati, H.; Sy, M.; Lo, B.; Boukheddaden, K. Isomorphism between the Electro-Elastic Modelling of the Spin Transition and Ising-like Model with Competing Interactions. *J. Appl. Phys.* **2021**, *129*, 153901. [CrossRef]
31. Ndiaye, M.; Boukheddaden, K. Electro-elastic Modelling of the Two-Step High-Spin to Low-Spin Relaxation with Transient Self-Organized Spin States in 2D Spin Crossover Solids. *J. Phys. Soc. Jpn.* **2020**, *89*, 014004. [CrossRef]
32. Nishino, M.; Yogendra, S.; Boukheddaden, K.; Miyashita, S. Tutorial on elastic interaction models for multistep spin-crossover. *J. Appl. Phys.* **2021**, *130*, 141102. [CrossRef]
33. Paez-Espejo, M.; Sy, M.; Boukheddaden, K. Elastic Frustration Causing Two-Step and Multistep Transitions in Spin-Crossover Solids: Emergence of Complex Antiferroelastic Structures. *J. Am. Chem. Soc.* **2016**, *138*, 3202–3210. [CrossRef]
34. Pillet, S.; Bendeif, E.-E.; Bonnet, S.; Shepherd, H.J.; Guionneau, P. Multimetastability, phototrapping, and thermal trapping of a metastable commensurate superstructure in a FeII spin-crossover compound. *Phys. Rev. B Condens. Matter Mater.* **2012**, *86*, 064106. [CrossRef]
35. Collet, E.; Watanabe, H.; Brefuel, N.; Palatinus, L.; Roudaut, L.; Toupet, L.; Tanaka, K.; Tu-chagues, J.-P.; Fertey, P.; Ravy, S.; et al. Aperiodic Spin State Ordering of Bistable Molecules and Its Photoinduced Erasing. *Phys. Rev. Lett.* **2012**, *109*, 257206. [CrossRef]
36. Milin, E.; Patinec, V.; Triki, S.; Bendeif, E.; Pillet, S.; Marchivie, M.; Chastanet, G.; Boukheddaden, K. Hidden Hysteresis Revealed by Photo-Switching in a Multi-Stable Two-Dimensional Hoffman-Like Spin-Crossover Metal-Organic Framework. *Inorg. Chem.* **2016**, *55*, 11652–11661. [CrossRef]
37. Bousseksou, A.; Nasser, J.; Linares, J.; Boukheddaden, K.; Varret, F. Ising-like model for the two-step spin-crossover. *J. Phys. I* **1992**, *2*, 1381–1403. [CrossRef]
38. Boukheddaden, K.; Linares, J.; Codjovi, E.; Varret, F.; Niel, V.; Real, J.A. Dynamical ising-like model for the two-step spin-crossover systems. *J. Appl. Phys.* **2003**, *93*, 7103–7105. [CrossRef]
39. Singh, Y.; Oubouchou, H.; Nishino, M.; Miyashita, S.; Boukheddaden, K. Elastic-frustration-driven unusual magnetoelastic properties in a switchable core-shell spin-crossover nanostructure. *Phys. Rev. B* **2020**, *101*, 054105. [CrossRef]
40. Affes, k.; Slimani, A.; Singh, Y.; Maalej, A.; Boukheddaden, K. Magnetoelastic properties of a spin-crossover membrane deposited on a substrate. *J. Phys. Cond. Matt.* **2020**, *32*, 255402. [CrossRef]
41. Singh, Y.; Affes, K.; Belmouri, N.-I.; Boukheddaden, K. Clamping of Spin-Crossover Solid Inducing Crystal Bending and Spatial Spin Organization. *Mater. Today Phys.* **2022**, *27*, 100842. [CrossRef]
42. Traiche, R.; Sy, M.; Boukheddaden, K. Elastic Frustration in 1D Spin-Crossover Chains: Evidence of Multi-Step Transitions and Self-Organizations of the Spin States. *J. Phys. Chem. C* **2018**, *122*, 4083–4096. [CrossRef]
43. Traiche, R.; Oubouchou, H.; Boukhedaden, K. Elastic Modeling of Two-Step Transitions in Sterically Frustrated 1D Binuclear Spin-Crossover Chains. *Symmetry* **2021**, *13*, 1836. [CrossRef]
44. Boukheddaden, K.; Traiche, R.; Oubouchou, H.; Linares, J. Multistep Relaxations in a Spin-Crossover Lattice with Defect: A Spatiotemporal Study of the Domain Propagation. *Magnetochemistry* **2016**, *2*, 17. [CrossRef]
45. Ndiaye, M.; Belmouri, N.; Linares, J.; Boukheddaden, K. Elastic Origin of the Unsymmetrical Thermal Hysteresis in Spin Crossover Materials: Evidence of Symmetry Breaking. *Symmetry* **2021**, *13*, 828. [CrossRef]
46. Di Scala, N.; Belmouri, N.; Paez-Espejo, M.; Boukheddaden, K. Explaining the origin of the orientation of the front transformation in spin-transition crystals. *Phys. Rev. B* **2022**, *106*, 144107. [CrossRef]
47. Affes, K.; Singh, Y.; Boukheddaden, K. Electro-Elastic Modeling of Thermal Spin Transition in Diluted Spin-Crossover Single Crystals. *Int. J. Mol. Sci.* **2022**, *23*, 13854. [CrossRef] [PubMed]
48. Miyashita, S.; Konishi, Y.; Nishino, M.; Tokoro, H.; Rikvold, P.A. Realization of the mean-field universality class in spin-crossover materials. *Phys. Rev. B Condens, Matter Mater. Phys.* **2008**, *77*, 014105. [CrossRef]
49. di Scala, N.; Belmouri, N.E.I.; Espejo, M.A.P.; Boukheddaden, K. Three-Dimensional Electroelastic Modeling of the Nucleation and Propagation of the Spin Domains in Spin-Crossover Materials. *Phys. Rev. B* **2022**, *106*, 014422. [CrossRef]
50. Decurtins, S.; Gutlich, P.; Kohler, C.P.; Spiering, H. New examples of light-induced excited spin state trapping (LIESST) in iron(II) spin-crossover systems. *J. Chem. Soc. Chem. Commun.* **1985**, *7*, 430–432. [CrossRef]
51. Desaix, A.; Roubeau, O.; Jeftić, J.; Haasnoot, J.G. Light-induced bistability in spin transition solids leading to thermal and optical hysteresis. *Eur. Phys. J. B–Condens. Matter Complex Syst.* **1998**, *6*, 183–193. [CrossRef]
52. Létard, J.F.; Guionneau, P.; Rabardel, L.; Howard, J.A.K.; Goeta, A.E.; Chasseau, D.; Kahn, O. Structural, Magnetic, and Photomagnetic Studies of a Mononuclear Iron(II) Derivative Exhibiting an Exceptionally Abrupt Spin Transition. Light-Induced Thermal Hysteresis Phenomenon. *Inorg. Chem.* **1998**, *37*, 4432–4441. [CrossRef]
53. Oke, T.D.; Ndiaye, M.; Hontinfinde, F.; Boukheddaden, K. Magnetic-field induced multi-step transitions in ferromagnetic spin-crossover solids within the BEG model. *Eur. Phys. J. B* **2021**, *94*, 38. [CrossRef]
54. Felts, A.C.; Cain, J.M.; Andrus, M.J.; Ahir, A.R.; Abboud, K.A.; Slimani, A.; Meisel, M.W.; Boukheddaden, K.; Talham, D.R. Control of the Speed of a Light-Induced Spin Transition through Mesoscale Core–Shell Architecture. *J. Am. Chem. Soc.* **2018**, *140*, 5814−5824. [CrossRef] [PubMed]
55. Sadhukhan, P.; Qi Wu, S.; Long, J.I.; Nakanishi, T. Manipulating electron redistribution to achieve electronic pyroelectricity in molecular [FeCo] crystals. *Nat. Commun.* **2021**, *12*, 4836. [CrossRef] [PubMed]
56. Carbonera, C.; Dei, A.; Létard, J.-F.; Sangregorio, C.; Sorace, L. Thermally and light-induced valence tautomeric transition in a dinuclear cobalt–tetraoxolene com-plex. *Angew. Chem. Int. Ed.* **2004**, *43*, 3136–3138. [CrossRef] [PubMed]

57. Schmidt, R.D.; Shultz, D.A.; Martin, J.D. Magnetic bistability in a cobalt bis (dioxo-lene) complex: Long-lived photoinduced valence tautomerism. *Inorg. Chem.* **2010**, *49*, 3162–3168. [CrossRef]
58. Tao, J.; Maruyama, H.; Sato, O. Valence tautomeric transitions with thermal hystere-sis around room temperature and photoinduced effects observed in a co-balt−tetraoxolene complex. *J. Am. Chem. Soc.* **2003**, *128*, 1790–1791. [CrossRef]